Barotropic Circulation around Islands with Friction*

LARRY PRATT AND JOSEPH PEDLOSKY

Woods Hole Oceanographic Institution, Woods Hole, Massachusetts

(Manuscript received 3 February 1997, in final form 5 January 1998)

ABSTRACT

Godfrey's *Island Rule* is generalized to include previously neglected dissipation on the north, south, and east boundaries of the island as well as the eastern basin boundary. The resulting extended island rule predicts the transport ψ_I between the island and the eastern basin boundary when strong frictional effects alter Godfrey's original result. The new result is derived for a barotropic ocean with either Munk or Stommel friction and with no bottom topography. The Munk case is marked by the interesting feature that friction enhances the flow over a certain range of widths of the gap separating the island from the western (or eastern) basin boundary. Transport predictions for the Munk case are compared to results based on linear and moderately nonlinear numerical simulations. The original island rule overpredicts ψ_I by no more than 25% unless the island is within about 3 Munk layer thickness of the east or west boundary, in which case the errors are much larger. For such cases the extended island rule is able to predict ψ_I within 10%, at least for the cases explored. The numerical simulations also show the transport enhancement predicted by the extended island rule. Implications for possible frictional blocking of the Indonesian Throughflow are discussed. The authors argue that middle-of-the-road estimates for δ_M suggest lateral friction as a serious candidate for the overestimate of the Indonesian Throughflow transport by the original island rule. Implications for the English Channel, the Mozambique Channel, and the Denmark Strait are discussed.

1. Introduction

The *Island Rule* (Godfrey 1989) and its extensions (Wajsowicz 1993, 1996; Pedlosky et al. 1997) provide for estimation of the wind-driven transport between an island and an eastern basin boundary on a beta plane. The most notable application is the indirect calculation of the Indo–Pacific transport through application of the island rule between Australia and South America, an estimate that yields a value of 12–15 Sv (Sv $\equiv 10^6$ m^3 s^{-1}). This value is moderately greater than most modern estimates (5–10 Sv) of the Indo–Pacific throughflow. (Wijffels et al. 1996). The rule is now being applied to other islands such as Hawaii (Qiu et al. 1997) and other applications are inevitable. In addition, analytical models of ocean circulation generally depend on the island rule to provide boundary conditions. For example, in a barotropic model with $\psi = 0$ along the basin's eastern boundary, where ψ is the transport stream function, the island rule provides for specification of $\psi = \psi_I$ on the island boundary. Errors in ψ_I may alter interior circulation features such as boundary currents, stagnation points, and recirculations to the point of distortion of the physics. Given the importance of Godfrey's result in both model and field studies, it is important to be able to anticipate success or failure of the rule in a given setting. The object of this work is to identify several common situations in which the island rule breaks down due to the presence of neglected frictional effects and to present an extended version of Godfrey's result that takes these effects into account.

To further motivate the work it is helpful to provide a brief sketch of the island rule and its underlying assumptions. Consider an island lying in a closed barotropic ocean, as shown in Fig. 1. The island rule can be obtained by applying the circulation theorem to the contour C, which runs around the island and extends to the eastern basin boundary, resulting in the following integral constraint:[1]

* Woods Hole Oceanographic Institution Contribution Number 9435.

Corresponding author address: Dr. Larry Pratt, WHOI, MS 21, 360 Woods Hole Rd., Woods Hole, MA 02543-1541.
E-mail: 1pratt@whoi.edu

[1] Equation (1.1) can be derived directly from the horizontal momentum equation written in the form

$$\frac{\partial \mathbf{u}}{\partial t} + (\zeta + f)\mathbf{k} \times \mathbf{u} = -\nabla\left(\frac{p}{\rho} + \frac{|\mathbf{u}|^2}{2}\right) + \text{diss}(\mathbf{u}) + \frac{\boldsymbol{\tau}}{\rho H}.$$

If the tangential component of this equation is integrated around C, the first term on the right-hand side drops out due to periodicity. The only remaining nonlinear term $\zeta \mathbf{k} \times \mathbf{u}$ leads to the vorticity flux term in (1.1). For an equivalent barotropic ocean in which the upper

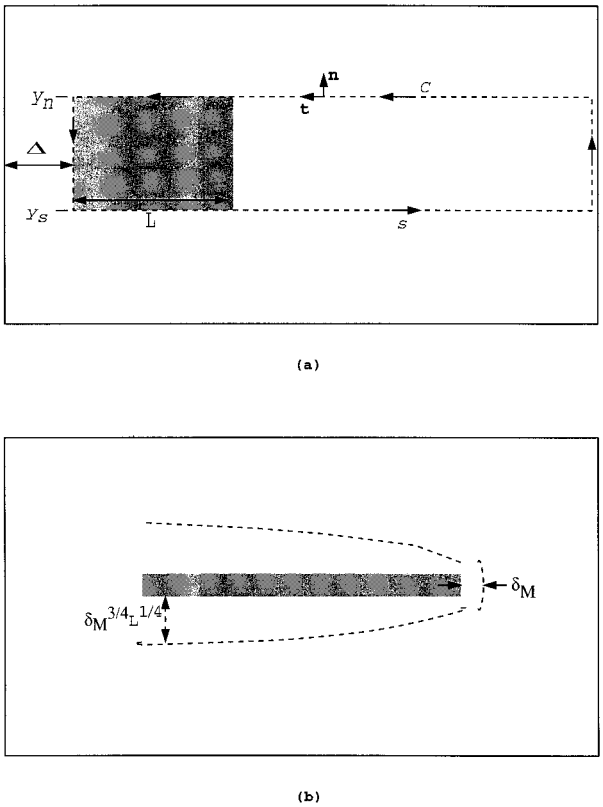

FIG. 1. Definition sketches showing (a) the island and the Godfrey integration circuit C and (b) a zonally elongated island with Munk layer on the east coast and diffusive boundary layers on the north and south coasts.

$$\beta(y_N - y_S)\psi_I = -\oint_C \frac{\boldsymbol{\tau}}{\rho}\cdot\mathbf{t}\, ds - \oint_C H\mathrm{diss}(\mathbf{u})\cdot\mathbf{t}\, ds + \oint_C H\mathbf{u}\zeta\cdot\mathbf{n}\, ds + \frac{\partial}{\partial t}\oint_C H\mathbf{u}\cdot\mathbf{t}\, ds. \tag{1.1}$$

Here **t** and **n** are unit tangent and normal vectors to the contour C, H is the depth, and $\oint_C ds$ represents the counterclockwise contour integration about C. Since the basin is closed, ψ_I is now the volume transport *around* the island: that is, the transport between the island and any basin boundary. Equation (1.1) expresses the balance between the vorticity input by the curl of the wind stress $\boldsymbol{\tau}$, the net flux of planetary vorticity across the contour C (left-hand term), frictional dissipation of vorticity (second term on the right), net flux of relative vorticity (third term on the right), and time variation of the total circulation about C (final term). In a linear, steady flow in which dissipation is weak about C, the final three terms in (1.1) are negligible and their omission leads to the island rule:

$$\psi_I = \frac{-\oint_C (\boldsymbol{\tau}/\rho)\cdot\mathbf{t}\, ds}{\beta(y_N - y_S)}. \tag{1.2}$$

The transport ψ_I can thus be estimated by calculating the integral of the tangential component of the wind stress about C. As shown by Wajsowicz (1993), the C integration can be thought of as the sum of an integration about the island itself and an integration about a circuit surrounding the ocean patch to the east of the island. The second integration gives a y-averaged Sverdrup transport to the east of the island, while the former gives the average transport $\overline{\psi}_W$ in the western boundary current flowing along the east coast of the island. Since the Sverdrup component could be calculated without knowledge of the shape or size of the island, or of reference to (1.2), $\overline{\psi}_W$ is the fundamental unknown removed by the island rule.

A key assumption in (1.2) is the neglect of dissipation and this is made plausible by Godfrey's choice of integration path, which avoids coastlines that might contain western boundary currents. In particular, frictional dissipation of vorticity around the island is assumed to occur primarily on its east coast and is assumed to be negligible over its north, south, and west coasts. Pedlosky et al. (1997, hereafter PPSH) explore a variety of island circulations on a barotropic beta plane using analytical and numerical techniques as well as laboratory experiments. In a series of numerical simulations based on the Munk model, and with various island shapes and forcings, the island rule is generally found to overestimate the actual ψ_I by a modest 0%–25%. Comparisons based on $\overline{\psi}_W$ yield moderately good agreement, with the island rule overestimating the actual value of $\overline{\psi}_W$ by, at most, 45%. In addition, it is found that the overestimate is primarily due to the presence of friction acting along the north and south boundaries of the island and, to a lesser extent, the west coast of the island and the east coast of the basin. Other possible sources of error, such as net relative vorticity fluxes due to eddy shedding, boundary layer separation, and other nonlinear processes are found to be of secondary importance.

In the study of PPSH, only two cases involving complete breakdown of (1.2) are noted. The first occurs when the island is narrow and zonally elongated (Fig. 1b), in which case frictional dissipation acting within weak boundary layers on the island's north and south coasts can surpass the contribution of the local wind stress. In this case, (1.2) is replaced by the requirement that the *net* dissipation around the island must vanish, a constraint that forms the basis for a modified transport prediction that can be formulated using a linear Munk or Stommel model. The transport predicted by the new rule is always less than that predicted by the original

layer is active and the lower layer inactive, the result is the same except that the vorticity flux is replaced by potential vorticity flux (Pedlosky et al. 1997).

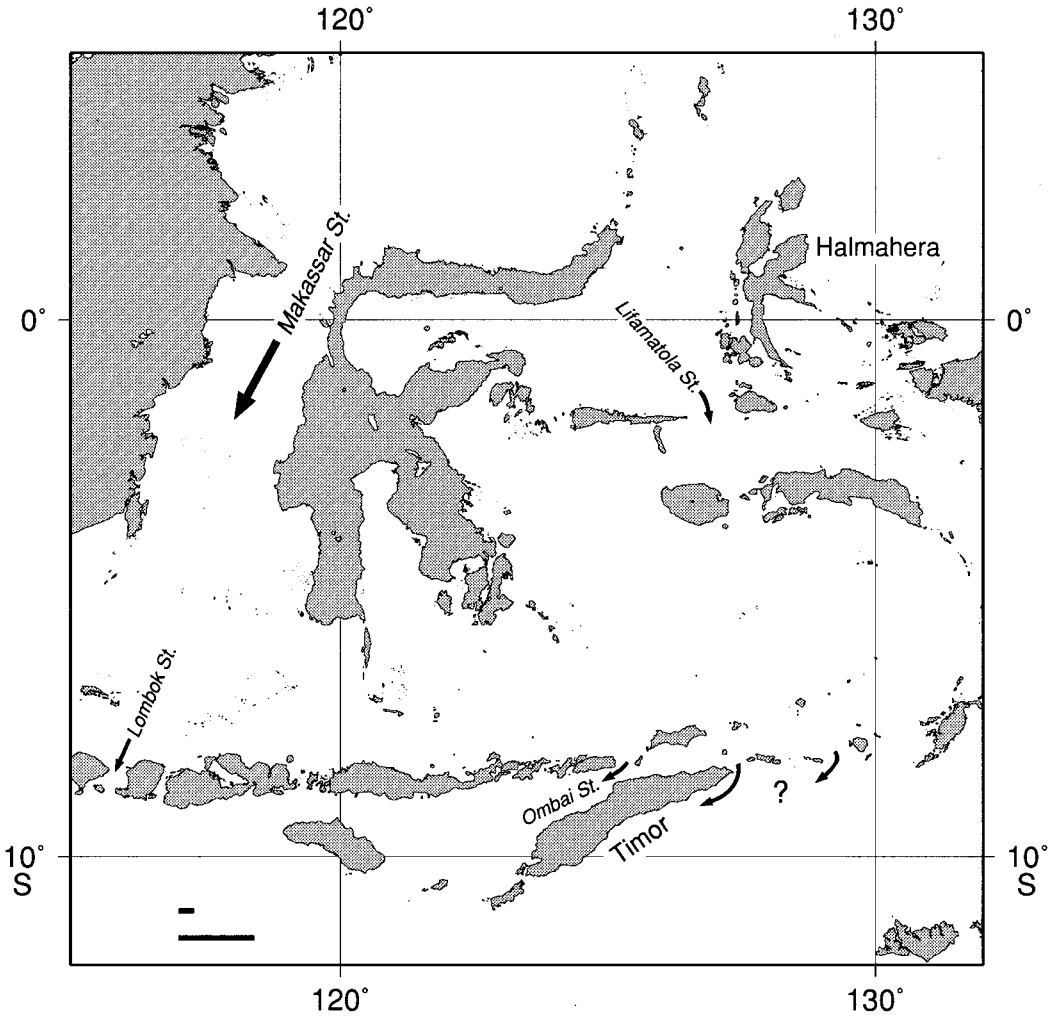

FIG. 2. The Indonesian seas. The two solid bars at the lower left show the range in Munk layer thickness as explained in section 7.

and, interestingly enough, the two predictions differ by a modest amount (at most, 20% in the case of the Munk model).

The second case of breakdown is more severe and occurs when the island is placed within the range of frictional influence of a basin boundary (Fig. 1a). The rule of thumb here is that when the width Δ of the gap separating the island from the basin is less than the appropriate frictional boundary layer thickness (in a Munk model: $\delta_M = (A_H/\beta)^{1/3}$, where A_H is the horizontal eddy viscosity), frictional blocking of the flow will reduce the transport below that predicted by the island rule. Wajsowicz (1993) has calculated the gap dissipation and modified the island rule accordingly for the case of proximity to a western boundary, a result that will be used later in this treatment. PPSH have examined the problem of proximity to a northern boundary numerically and have noted a significant reduction of the transport when the gap thickness Δ becomes less than $1.5\delta_M\alpha^{1/3}$, where $\alpha = L/(y_N - y_S)$ is the island aspect ratio. These calculations would seem to have particular relevance to the Indonesian Throughflow (Fig. 2), where the currents must navigate gaps that may well be narrower than the appropriate frictional length scale. We examine this issue more carefully in section 7.

The purpose of this work is to extend the island rule to include the effects of frictional dissipation on the coastal boundaries touched by the ''Godfrey'' integration circuit *C*. The aim is to obtain an extended island rule that will account for frictional modifications in the total transport when the island is separated from the mainland by a thin gap. The extended rule should be expected to apply with some precision in analytical or laboratory models, where the friction coefficients are known. In the ocean, where parameterizations of friction yield coefficients that are known only within a broad range, our calculations provide the maximum gap thickness below which the flow *might* be impeded and rough estimates of how much the transport is reduced. The emphasis will be on flows with lateral (Munk) friction

only, although the extended rule will also be written down for a model with bottom (Stommel) friction. This preference is due in part to the more interesting character of results from the Munk model and also to the fact that the bulk of the Indonesian Throughflow is confined to the upper 400 m of the water column and presumably insulated from the bottom over much of its path. Section 2 begins with a treatment of friction along the western edge of the island based on the calculation of Wajsowicz (1993). This case is particularly important when the island lies close to a western basin boundary. Her result is generalized to include possible proximity to an eastern basin boundary. An interesting development here is that friction actually enhances ψ_I over an intermediate range in eastern or western gap thicknesses. Section 3 considers the effects of friction on the island's northern and southern boundaries, a problem requiring analysis of diffusive boundary layers (Fig. 1b) that arise there. When combined with the results of Section 2, this calculation gives rise to the extended island rule.

Simulations of barotropic flow around an island based on a barotropic, primitive equation numerical model are then presented (Section 4) and comparison with the extended island rule are made over a range spanning linear to moderately nonlinear dynamics. An important quantity in this comparison is ratio of predicted and calculated values of $\overline{\psi}_W$ and this is discussed in Section 5. Section 6 contains a statement of the extended island rule for a Stommel model. Finally, Section 7 discusses ramifications of the calculations for the Indonesian seas, the conclusion being that the widths of the individual passages are probably small enough to frictionally impede the throughflow.

In the text that follows all references to the island rule or the original island rule will mean Eq. (1.2). References to the extended island rule will refer to the formulas obtained here [cf. (3.7) or (6.1)] and should not be confused with other extensions of the island rule, such as that of Wajsowicz (1993) to multiple islands. Finally, the term ''dissipation'' refers to vorticity (and not energy) dissipation, as defined within the circulation theorem. For instance, the dissipation term in (1.1) corresponding to an ocean with lateral friction would be

$$\oint_C \text{diss}(\mathbf{u})\cdot\mathbf{t}\, ds = A_H \oint_C \mathbf{t}\cdot\nabla^2\mathbf{u}\, ds, \qquad (1.3)$$

where A_H is the horizontal viscosity.

2. Frictional effects in meridional gaps

Figure 3a contains a definition sketch showing the model basin and islands, both of which are rectangular, as well as dimensions and coordinate origins. It is now assumed that the dynamics are linear, which requires the appropriate frictional boundary layer thickness to be much larger than the inertial thickness $\delta_I = (U/\beta)^{1/2}$, where U is a velocity scale based on a Sverdrup

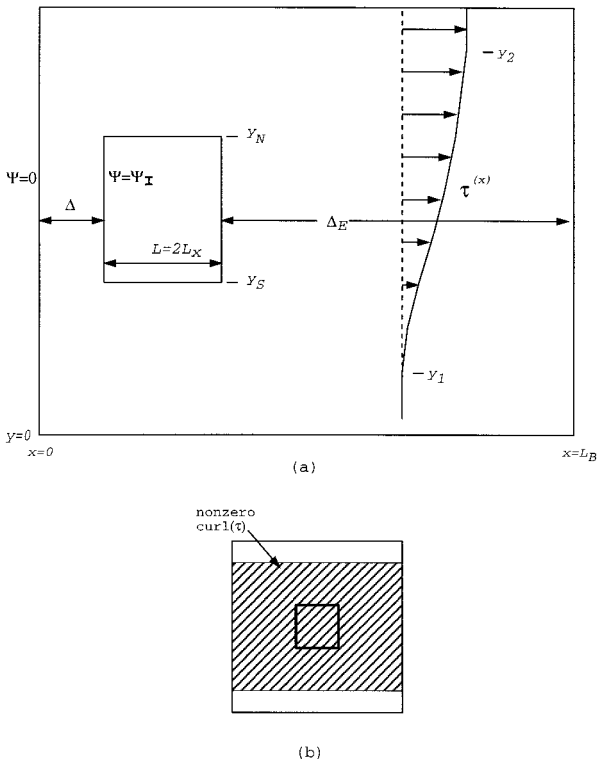

FIG. 3. Definition sketches showing the wind stress distribution and the island dimensions.

interior flow. Then frictional effects along solid boundaries can be symbolically appended to (1.2) by writing

$$\beta(y_N - y_S)\psi_I = -\oint_C \frac{\boldsymbol{\tau}}{\rho}\cdot\mathbf{t}\, ds - D_W - D_N - D_S - D_E, \qquad (2.1)$$

where D_W, D_N and D_S represents depth integrated dissipation along the western, northern, and southern coasts of the island, and D_E represents depth integrated dissipation along the segment of C lying along the eastern basin boundary.

a. The gap to the west of the island

First consider the dissipation in the gap to the west of the island. As shown in Fig. 3a, the gap width is denoted by Δ and the island extends meridionally from y_N to y_S. If $\Delta/(y_N - y_S) \ll 1$, then the meridional velocity component v should dominate the zonal velocity component u in the gap and, therefore, $\partial/\partial x$ should be $\gg \partial/\partial y$. The gap flow should therefore be governed by western boundary layer equations used in connection with Munk or Stommel models (Pedlosky 1996). In the case of a Munk model, the appropriate vorticity equation is

$$\psi_{xxxx} - \delta_M^{-3}\psi_x = -\frac{1}{A_H}\text{curl}\left(\frac{\boldsymbol{\tau}}{\rho}\right), \qquad (2.2)$$

where ψ is the transport streamfunction ($\partial\psi/\partial x = vH$ and $\partial\psi/\partial y = -uH$), $\boldsymbol{\tau}$ is the surface wind stress, and H is the (constant) depth. The wind stress term in (2.2) gives rise to a Sverdrup flow in the gap that is smaller than the total gap transport by $O(\delta_M/L_B)$, where L_B is the basin width. Neglect of the right-hand side would appear, therefore, to lead to negligible error. Wajsowicz (1993) solved the resulting homogeneous equation subject to the boundary conditions

$$\psi(0, y) = 0 \tag{2.3a}$$

$$(\partial\psi/\partial x)_{x=0} = 0 \tag{2.3b}$$

$$\psi(\Delta, y) = \psi_I \tag{2.3c}$$

$$(\partial\psi/\partial x)_{x=\Delta} = 0. \tag{2.3d}$$

She then used the solution to calculate the dissipation term D_W in (2.1) and extend the island rule accordingly. In order to point out some interesting and previously unrevealed behavior this calculation is now described in more detail.

Solving the homogeneous form of (2.2) subject to (2.3a–d) leads to

$$\psi(x, y) = c_1 + c_2 e^{x/\delta_M} + c_3 \cos\left(\frac{\sqrt{3}\,x}{2\delta_M}\right) e^{-x/2\delta_M} + c_4 \sin\left(\frac{\sqrt{3}\,x}{2\delta_M}\right) e^{-x/2\delta_M}, \tag{2.4}$$

where

$$c_1 = \frac{\gamma_1(\Delta)\psi_I}{\gamma_1(\Delta) + \gamma_2(\Delta)},$$

$$c_3 = \frac{\left[-\gamma_1(\Delta) - \frac{2}{\sqrt{3}} \sin\left(\frac{\sqrt{3}\,\Delta}{2\delta_M}\right) e^{-\Delta/2\delta_M}\right]\psi_I}{\gamma_1(\Delta) + \gamma_2(\Delta)} \tag{2.5a}$$

$$c_4 = \frac{\left[-\frac{1}{\sqrt{3}}\gamma_1(\Delta) - 2 \sin\left(\frac{\sqrt{3}\,\Delta}{2\delta_M}\right) e^{-\Delta/2\delta_M}\right]\psi_I}{\gamma_1(\Delta) + \gamma_2(\Delta)},$$

$$c_2 = \frac{1}{2}c_3 - \frac{\sqrt{3}}{2}c_4 \tag{2.5b}$$

and

$$\gamma_1 = \left[\cos\left(\frac{\sqrt{3}\,\Delta}{2\delta_M}\right) - \sqrt{3}\sin\left(\frac{\sqrt{3}\,\Delta}{2\delta_M}\right)\right] e^{-\Delta/2\delta_M} - e^{\Delta/\delta_M} \tag{2.6a}$$

$$\gamma_2 = \left[\cos\left(\frac{\sqrt{3}\,\Delta}{2\delta_M}\right) + \sqrt{3}\sin\left(\frac{\sqrt{3}\,\Delta}{2\delta_M}\right)\right] e^{\Delta/2\delta_M} - e^{-\Delta/\delta_M}. \tag{2.6b}$$

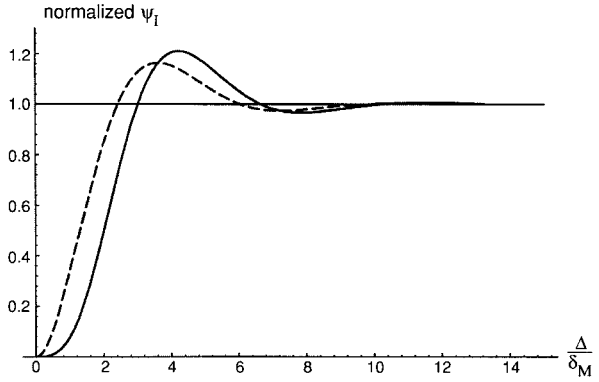

FIG. 4. The total transport around the island ψ_I, normalized by the transport predicted by Godfrey's island rule (1.2) and plotted as a function of the dimensionless gap width. The solid curve is obtained from the formula of Wajsowicz [1993, her Eq. (4.4)], here Eq. (2.8), and shows the result obtained by extending the island rule to include friction within the gap to the west of the island. The effects of friction due to Sverdrup flow in the gap are not included. The dashed curve shows the transport stream function for a Munk layer along the western basin boundary that is undisturbed by the island. For this curve the horizontal axis should be interpreted as x/δ_M.

In a Munk model the depth-integrated dissipation term D_W is the integral with respect to y of the boundary friction $HA_H\partial^2 v/\partial x^2$ from the northwest to southwest corner of the island [cf. Eq. (1.3)]. Simplifying the integration is the fact that the homogeneous gap solution is independent of y [an advantage that disappears when the wind stress term is included in Eq. (2.2)]. Using (2.4)–(2.6) to calculate $(\partial^2 v/\partial x^2)_{x=\Delta}$ and multiplying the result by the boundary length $(y_N - y_S)$ leads to evaluation of the island western boundary dissipation as

$$D_W = -HA_H(y_N - y_S)(\partial^2 v/\partial x^2)_{x=\Delta} = -\frac{(y_N - y_S)\beta\gamma_2(\Delta)}{(\gamma_1(\Delta) + \gamma_2(\Delta))}\psi_I. \tag{2.7}$$

Substituting this expression into (2.1) and ignoring (for the time being), the remaining dissipation terms leads to

$$\psi_I = \frac{-\oint_C (\boldsymbol{\tau}/\rho)\cdot\mathbf{t}\, ds}{\beta(y_N - y_S)} \frac{(\gamma_1(\Delta) + \gamma_2(\Delta))}{\gamma_1(\Delta)}, \tag{2.8}$$

which is equivalent to Eq. (4.4) of Wajsowicz (1993).

According to (2.8), the ratio of the transport through the gap to the value predicted by the original island rule is $[\gamma_1(\Delta) + \gamma_2(\Delta)]/\gamma_1(\Delta)$ and a plot of this function reveals an interesting behavior. As shown by the solid curve in Fig. 4, the value of ψ_I matches that predicted by island rule (the horizontal solid line) for sufficiently large gap widths: $\Delta \gg \delta_M$. As Δ/δ_M is reduced to zero, the flow becomes completely blocked ($\psi_I = 0$), as expected. However, an intermediate range exists ($3.0 < \Delta/\delta_M < 6.7$) where ψ_I is actually greater than that predicted by the island rule.

It is remarkable that friction in the gap should enhance the transport, but the situation can be rendered more plausible by examination of the velocity structure of the boundary layer solution. The dashed line in Fig. 4 shows the streamfunction one would obtain from a Munk layer solution in a semi-infinite ocean with no island. In viewing this curve, one should interpret the horizontal axis as x/δ_M, rather than Δ/δ_M. The solution is obtained from (2.4)–(2.6) by letting Δ/δ_M tend toward ∞. The dashed curve has a maximum at $y/\delta_M \cong 3.6$ and a minimum at $y/\delta_M \cong 7.3$, indicating reversals of the meridional velocity. That is, the boundary layer carries a unidirectional flow within 3.6 Munk layer thicknesses of the western boundary, with a band of reverse flow farther offshore. The total transport in the nearshore band is thereby larger than the boundary layer transport as a whole. When the island is positioned so as to impede the reverse flow, but not the direct flow, the total transport through the gap is larger than what is carried by the boundary layer as a whole. There are some additional subtleties, as evidenced by the fact that the dashed and solid curves do not quite have the same zero crossings, but this explanation seems to account for much of the observed behavior.

Figures 5a–c show meridional velocity profiles based on (2.4) in the gap for decreasing dimensionless gap thickness. In the case of Fig. 5a ($\Delta/\delta_M = 6$), a flow reversal exists in the eastern sector of the gap. In Fig. 5b, Δ/δ_M has been decreased to 4, resulting in blockage of all the reverse flow and an increase in the normalized value of ψ_I. In fact, Fig. 4 shows that the dimensionless ψ_I reaches its maximum value at about $\Delta/\delta_M = 4$. Finally, Fig. 5c shows the result of decreasing Δ/δ_M to 2, namely, a nearly symmetrical profile. Note that the curvature of the velocity at the eastern edge of the gap is of opposite sign from that of the Fig. 5b curve, indicating opposite signs of vorticity dissipation. In the former, the dissipation retards the circulation while in the former the circulation is enhanced.

Finally, it is noted that the transport maximum is a peculiarity of the Munk problem: the Stommel boundary layer velocity decays monotonically from the western wall and the gap transport is therefore monotonically reduced to zero as Δ tends to zero.

b. The gap to the east of the island

The above result can easily be extended to include the case of proximity of the island to an eastern basin boundary. Denoting the eastern gap thickness by Δ_E and redefining $x = 0$ to correspond to the eastern boundary of the island, it can easily be shown that the solution to (2.2) is obtained by replacing ψ_I by $-\psi_I$ in (2.4) and adding ψ_I to the resulting formula. From this the dissipation arising along the eastern portion of the circuit C can be calculated with the result

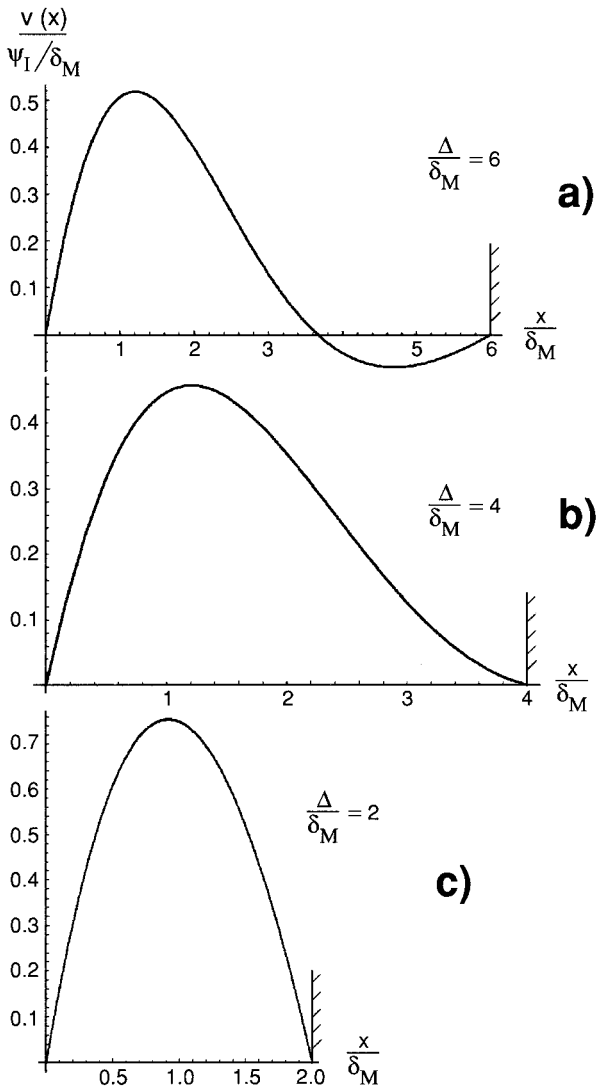

FIG. 5. Dimensionless velocity profiles in the gap to the west of the island for (a) $\Delta/\delta_M = 6$, (b) $\Delta/\delta_M = 4$, and (c) $\Delta/\delta_M = 2$, all calculated using Eq. (2.4).

$$D_E = HA_H(y_N - y_S)(\partial^2 v/\delta x^2)_{x=\Delta_E} = -\frac{(y_N - y_S)\beta\gamma_2(\Delta_E)}{\gamma_1(\Delta_E) + \gamma_2(\Delta_E)}\psi_I. \tag{2.9}$$

Including this additional term in (2.1) leads to an extended version of (2.8), namely,

$$\psi_I = \frac{-\oint_C (\tau/\rho)\cdot\mathbf{t}\, ds}{\beta(y_N - y_S)\left(\dfrac{\gamma_1(\Delta)}{\gamma_1(\Delta) + \gamma_2(\Delta)} - \dfrac{\gamma_2(\Delta_E)}{\gamma_1(\Delta_E) + \gamma_2(\Delta_E)}\right)}. \tag{2.10}$$

Figure 6 shows the variation of the above transport function, again normalized by the island rule transport,

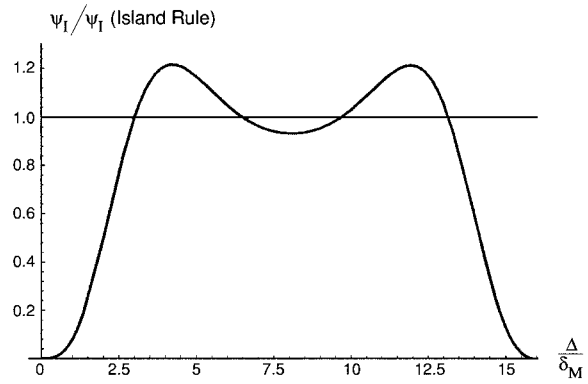

FIG. 6. The total transport around the island ψ_I, normalized by the transport predicted by Godfrey's island rule, as a function of dimensionless gap width when the island is moved across the entire basin. The curve is obtained by extending the island rule to include frictional effects on both the island's western boundary and the basin's eastern boundary due to narrow gap effects [cf. Eq. (2.10)]. Frictional effects caused by Sverdrup transport are not included, nor are frictional effects along the north or south boundaries of the island. The curve was obtained using a basin width of $20\delta_M$ and an island width $L = 3.9\delta_M$. The axis of symmetry ($\Delta/\delta_M = 8.05$) corresponds to having the island midway between east and west basin boundaries.

as the island is moved across the entire width of the basin. The plot is made using a basin width of $20\delta_M$ and an island width L of $3.8\delta_M$, which is a case explored numerically later. The curve shows the symmetrical influence of friction between the eastern and western gaps. (The axis of symmetry $\Delta/\delta_M = 8.1$ corresponds to the gap thickness at which the island is midway across the basin.)

c. *Friction resulting from inclusion of the Sverdrup flow*

There is one remaining source of friction on the western island boundary that is generally minor. It arises from the presence of Sverdrup flow along the western island boundary and the need for the meridional Sverdrup velocity to be brought to zero at this boundary. By considering only the homogeneous solution to (2.2) we have neglected this effect. For narrow gaps the Sverdrup velocity is overwhelmed by the velocity of fluid being squeezed through the gap, and the corresponding frictional effects are weak in comparison. For wide gaps ($\Delta/\delta_M \gg 1$) the effect remains finite but generally small compared to the other terms in the circulation integral. In this case a local boundary correction,

$$\psi'(x, y) = \beta^{-1}\left[(x - \Delta)\mathrm{curl}\left(\frac{\boldsymbol{\tau}}{\rho}\right) - \delta_M \mathrm{curl}\left(\frac{\boldsymbol{\tau}}{\rho}\right)e^{-(\Delta - x)/\delta_M}\right]$$

can be added to the gap solution (2.4). The associated dissipation term, which must be appended to D_W, is

$$\int_{y_S}^{y_N} \delta_M \mathrm{curl}\left(\frac{\boldsymbol{\tau}}{\rho}\right)_{x=\Delta} dy. \tag{2.11a}$$

A similar effect occurs along the eastern boundary of the basin, and the corresponding dissipation term

$$-\int_{y_S}^{y_N} \delta_M \mathrm{curl}\left(\frac{\boldsymbol{\tau}}{\rho}\right)_{x=L_B} dy \tag{2.11b}$$

must be added to D_E.

As indicated above, these expressions are valid as long as the gap is wide (Δ or Δ_E is $\gg\delta_M$). When Δ or Δ_M is $O(\delta_M)$, the expressions are invalid; however, the frictional effects due to the contact of the wall with the (homogeneous) western boundary layer are larger by a factor L_B/δ_M than those due to the Sverdrup flow. Thus, we may simply retain (2.11a,b) in the circulation integral for all gap thicknesses without incurring serious error. Also note that the sum of (2.11a) and (2.11b) is zero if the wind stress curl is independent of x.

Supplementing D_W and D_E in (2.1) by the above amounts leads to

$$\psi_I = \frac{-\oint_C (\boldsymbol{\tau}/\rho)\cdot\mathbf{t}\, ds - \delta_M \int_{y_S}^{y_N}\left[\mathrm{curl}\left(\frac{\boldsymbol{\tau}}{\rho}\right)_{x=\Delta} - \mathrm{curl}\left(\frac{\boldsymbol{\tau}}{\rho}\right)_{x=L_B}\right] dy}{\beta(y_N - y_S)\left[\dfrac{\gamma_1(\Delta)}{\gamma_1(\Delta) + \gamma_2(\Delta)} - \dfrac{\gamma_2(\Delta_E)}{\gamma_1(\Delta_E) + \gamma_2(\Delta_E)}\right]}. \tag{2.12}$$

3. The diffusive boundary layers on the north and south coasts of the island

The western boundary current along the island's east coast generally has finite transport at the north and south extremities, y_N and y_S, of that coast. According to linear theory, the flow there must turn the corners and must join with diffusive boundary layers along the island's north and south coasts. The diffusive boundary layers are the same as those that would occur along a northern or southern basin boundary in a linear Munk or Stommel model. In either case, the

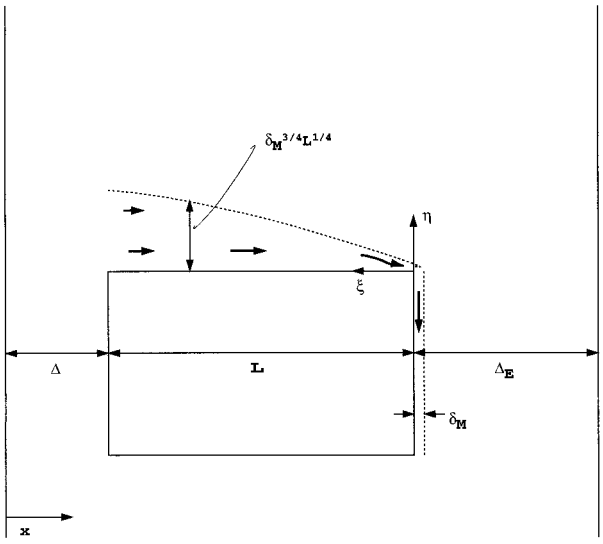

FIG. 7. Definition sketch for northern boundary layer calculation.

boundary layers tend to broaden as one moves in the westward direction, the thickness varying as $\delta_S^{1/2}(\Delta + L - x)^{1/2}$ in a Stommel model and $\delta_M^{3/4}(\Delta + L - x)^{1/4}$ in a Munk model, where $\Delta + L - x$ is the westward distance from the corner. These features are documeted in PPSH, and the Stommel version of the boundary layer is analyzed in order to calculate the dissipation terms D_S and D_N in (2.1). It is also shown that decreasing the length $y_N - y_S$ below the mean boundary layer thickness $\delta_S^{1/2}(\Delta + x - L)^{1/2}$ leads to a situation in which D_S and D_N dominate the dissipation in the western boundary layer. Under these conditions, the assumptions behind the original island rule completely break down as the dominant terms in the circulation integral change. However, a modified formula for ψ_I can be found that, quite surprisingly, gives only a slightly different transport estimate. A modified rule is also written down, without derivation, for the case of Munk dynamics and an infinitesimally thin island. The purpose of this section is to calculate the dissipation terms D_S and D_N for an island of finite width and combine the results with those of section 2 in order to complete the extended island rule for the Munk problem.

For islands of more general (and realistic) shapes the analysis presented here will be pertinent over a portion of the island perimeter. That portion consists of any stretch of coastline that does not deviate more than a characteristic boundary layer thickness ($\delta_M^{3/4}L^{1/4}$) over the length L. So, for example in Fig. 2, the nearly zonally oriented feature east of the Makassar Strait and, farther south, the Indonesian Archipelago itself would qualify.

For illustrative purposes, such stretches are encountered only along the northern and southern boundaries of our idealized island. Consider the boundary current on the north coast of the island, as shown schematically in Fig. 7. The flow direction shown is eastward, but this is not important to the overall problem. To the north of the boundary layer exists a Sverdrup regime characterized by transport streamfunction ψ^S such that $\partial\psi^S/\partial x = \beta^{-1}\,\mathrm{curl}(\boldsymbol{\tau}/\rho)$. On the boundary itself the value of the streamfunction is ψ_I. One may also anticipate from the above remarks that the appropriate boundary layer coordinates are the dimensionless distances ξ and η from the northeast corner of the island:

$$\xi = \frac{\Delta + L - x}{L}$$

and

$$\eta = \frac{y - y_N}{\delta_M^{3/4}L^{1/4}}.$$

The streamfunction is now partitioned as $\psi(x, y) = \psi^S(x, y) + \phi(\xi, \eta)$ and substitution into the barotropic potential vorticity equation

$$\beta\psi_x = \mathrm{curl}(\boldsymbol{\tau}/\rho) + A_H\nabla^4\psi,$$

leads, to lowest order, to the boundary layer equation

$$-\phi_\xi = \phi_{\eta\eta\eta\eta}. \tag{3.1}$$

The boundary conditions are

$$\phi(\xi, 0) = \psi_I - \psi^S(x, y_N) \tag{3.2a}$$

$$\phi_\eta(\xi, 0) = 0 \tag{3.2b}$$

$$\lim_{\eta\to\infty} \phi(\xi, \eta) \to 0 \tag{3.2c}$$

$$\phi(0, \eta)_{\eta>0} = 0. \tag{3.2d}$$

These reflect the conditions of no normal flow and no slip at the northern boundary and of merger with the Sverdrup interior. The final condition is more subtle and arises out of consideration of the merger at the northeast island corner between the northern boundary layer and the Munk boundary layer on the island's eastern wall. Since the scale thickness of the former ($\delta_M^{1/4}L^{3/4}$) is asymptotically larger than the thickness of the larger (δ_M), the actual thickness of the former must tend to zero as the northeast corner is approached from the west. There the northern boundary layer becomes an infinitesimally thin flow that turns the corner and feeds the Munk layer. At any nonzero distance north of the corner ($\eta > 0$), Sverdrup conditions pertain and thus ϕ must = 0 there.

The problem posed by (3.1) and (3.2) can be solved using the Laplace transform:

$$\Phi(t, \eta) = \int_0^\infty e^{-t\xi}\phi(\xi, \eta)\, d\xi.$$

Taking the transform of (3.1) and using (3.2d) leads to

$$-t\Phi = \Phi_{\eta\eta\eta\eta},$$

and the solution to this equation satisfying $\lim_{\eta\to\infty}\Phi = 0$ is

$$\Phi = Ae^{-t^{1/4}\eta/\sqrt{2}}\left(\cos\frac{t^{1/4}\eta}{\sqrt{2}} + \sin\frac{t^{1/4}\eta}{\sqrt{2}}\right). \quad (3.3)$$

Satisfaction of the remaining boundary conditions is considerably simplified if it is assumed that the wind stress curl depends only on y. In this case, the the Sverdrup streamfunction that satisfies the condition of no normal flow on the basin's eastern boundary is $\psi^S = -\beta^{-1}(L\xi + \Delta_E)\,\mathrm{curl}(\boldsymbol{\tau}/\rho)_{y=y_N}$. Using this expression, the Laplace transform of (3.2a) can be evaluated easily, with the result

$$\Phi(\xi, 0) = \frac{(\psi_I + \beta^{-1}\Delta_E \mathrm{curl}(\boldsymbol{\tau}/\rho)_{y=y_N})}{t} + \frac{L\,\mathrm{curl}(\boldsymbol{\tau}/\rho)_{y=y_N}}{\beta t^2}.$$

With this condition and (3.2b), the coefficient A in (3.3) can be evaluated and the inverse transform applied to obtain

$$\phi(\xi, \eta) = \frac{1}{2\pi i}\int_{-i\infty}^{i\infty}\left(\frac{\psi_I + \beta^{-1}\Delta_E \mathrm{curl}(\boldsymbol{\tau}/\rho)_{y=y_N}}{t} + \frac{L\,\mathrm{curl}(\boldsymbol{\tau}/\rho)_{y=y_N}}{\beta t^2}\right)\exp\left(\frac{t^{1/4}\eta}{\sqrt{2}} + t\xi\right)\left(\cos\frac{t^{1/4}\eta}{\sqrt{2}} + \sin\frac{t^{1/4}\eta}{\sqrt{2}}\right) dt. \quad (3.4)$$

In order to compute the dissipation term $D_N = A_H H \int_{L+\Delta}^{\Delta} u_{yy}\,dx$ it is not necessary to evaluate the above integral. Instead, (3.4) may be differentiated with respect to η three times and the result applied at $\eta = 0$, which gives $(\delta_M^{3/4}L^{1/4})^3 H u_{yy}$ at $y = y_N$. The integral that appears in this expression may be evaluated using the inverse transforms listed on p. 238 of Erdelyi (1954). Using the result to evaluate D_N gives

$$D_N = \int_{L+\Delta}^{\Delta} HA_H(u_{yy})_{y=y_N}\,ds = \kappa\left[\beta\psi_I + \left(\Delta_E + \frac{4}{5}L\right)\mathrm{curl}(\boldsymbol{\tau}/\rho)_{y=y_N}\right], \quad (3.5)$$

where $\kappa = (1.560\cdots)\delta_M^{3/4}L^{1/4}$. At the southern boundary a similar expression is obtained with y_N replaced by y_S, and thus

$$D_S = \kappa\left[\beta\psi_I + \left(\Delta_E + \frac{4}{5}L\right)\mathrm{curl}(\boldsymbol{\tau}/\rho)_{y=y_S}\right]. \quad (3.6)$$

All of the dissipation terms in (2.1) have now been evaluated and substitution into that equation leads, after some rearrangment, to the extended island rule:

$$\psi_I = \frac{-\oint_C (\boldsymbol{\tau}/\rho)\cdot\mathbf{t}\,ds - \delta_M\int_{y_S}^{y_N}\left[\mathrm{curl}\left(\frac{\boldsymbol{\tau}}{\rho}\right)_{x=\Delta} - \mathrm{curl}\left(\frac{\boldsymbol{\tau}}{\rho}\right)_{x=L_B}\right]dy - \kappa\left(\frac{4}{5}L + \Delta_E\right)(\mathrm{curl}(\boldsymbol{\tau}/\rho)_{y=y_N} + \mathrm{curl}(\boldsymbol{\tau}/\rho)_{y=y_S})}{\beta\left\{(y_N - y_S)\left[\frac{\gamma_1(\Delta)}{\gamma_1(\Delta) + \gamma_2(\Delta)} - \frac{\gamma_2(\Delta_E)}{\gamma_1(\Delta_E) + \gamma_2(\Delta_E)}\right] + 2\kappa\right\}}. \quad (3.7)$$

The assumptions of x-independent wind stress and constant-y north and south island boundaries has been made to simplify evaluation of the Laplace transforms in the derivation of the diffusive boundary layer solutions. Variable wind stress and boundary location may be formally included in these derivations but the resulting dissipation terms D_S and D_N will then become much more complicated. We have limited discussion to the simplest case as it provides most of the physical intuition that is likely to be gained from a more general calculation.

Equation (3.7) accounts for frictional effects along all solid boundaries touched by the integration contour C. It is also natural to ask how significant the dissipation is along the free sections of C, particularly where the island's western boundary is crossed. In view of (1.3) the corresponding contribution to the circulation integral is obtained by integrating $\delta_M A_H H\nabla^2 u$ along the segments of C that cross the gap to the east of the island. The term $\nabla^2 u$ is dominated by the component $\partial^2 u/\partial x^2 = -\partial^3\psi/(\partial y\partial x^2)$, at least in the vicinity of the western boundary layer. However, integration over the eastern gap leads to $[\partial^2\psi/\delta x\delta y]_{x=\Delta+L}^{x=L_B} = [\partial v/\delta y]_{x=\Delta+L}^{x=L_B}$, which is zero due to the no-slip boundary conditions. The remaining dissipation term is proportional to $\partial^2 u/\partial y^2$ and can generally be shown to be

negligible compared to the solid-wall dissipation terms.[2]

4. Numerical simulations

The extended island rule (3.7) has been tested using numerical solutions based on the Miami Isopycnic Coordinate Ocean Model (MICOM), documented by Bleck et al. (1992). The model has been configured for barotropic β-plane dynamics as described by PPSH (section 4a) and is forced by the wind stress distribution

$$\tau^{(x)} = \begin{cases} \tau_{o,} & (y \geq y_2) \\ \dfrac{\tau_o}{2}\left\{1 + \cos\left[\dfrac{\pi(y_2 - y)}{y_2 - y_1}\right]\right\}, & (y_1 \leq y \leq y_2) \\ 0, & \text{otherwise} \end{cases} \tag{4.1}$$

and $\tau^{(y)} = 0$. As shown in Figs. 3a and 3b, the wind stress curl is independent of x and is finite only in a latitude band extending from y_1 to y_2. Within that band the curl of τ is single signed and, for the experiments that follow, always anticyclonic. The model contains horizontal friction but no bottom friction. The general procedure is to choose a particular wind stress distribution and island shape and size, and then spin up a steady circulation from rest. A series of such runs is performed in which the western gap width Δ is varied. In addition to Δ/δ_M, a parameter of essential importance is the ratio of δ_M to the inertial thickness $\delta_I = (U/\beta)^{1/2}$, where U is a velocity scale based on the Sverdrup interior flow. {For the wind stress defined by (4.1), $\delta_I = [\tau_0/\rho\beta^2 H(y_1 - y_2)]^{1/2}$.} The ratio δ_I/δ_M is a measure of nonlinearity in the western boundary layers. A square basin of dimensions $0 < x < 2000$ and $0 < y < 2000$ km is used and the limits of the band of wind stress variation are fixed at $y = 300$ and $y_2 = 1700$ km. Finally, the island is centered at the latitude $y = 1000$ of maximum wind stress curl.

The barotropic version of the MICOM model solves for the free surface height, and there is no need to independently specify the pressure on the island. Thus ψ_I is determined without direct reference to the island rule or any related integral constraints. [In a rigid lid model, the value of ψ_I must typically be determined at each time step by requiring that the integral of the dissipation around the island boundary is zero (Kamenkovitch 1962; Bryan 1969).] In addition, the grid spacing and Munk layer thickness are fixed at 20 km and 100 km so that all frictional boundary layers are well resolved. Tests of numerical accuracy against a linear, analytical solution were performed by PPSH (see their section 5iii), and agreement with the predicted ψ_I within 1% was found for sufficiently small δ_I.

Figure 8a shows a reference calculation with a 380 km by 800 km island, $\delta_I = 20$ km, $\delta_M = 100$ km, and $\Delta = 600$ km. Since δ_I/δ_M is only 1/5, the dynamics are relatively linear. To the east of the island lies a rather broad, southward[3] Munk layer and, farther east, a southward Sverdrup flow. The flow in the Munk layer turns the corner without separation and continues westward along the south edge of the island. Upon reaching the western edge of the island, the boundary flow detaches and continues on to the western basin boundary where it is absorbed into a northward Munk layer. In the eastern portion of the gap separating the island from this western boundary lies a band of southward flow similar to that of the Fig. 5a velocity profile (which also has $\Delta/\delta_M = 6$). The original island rule [Eq. (1.2)] estimate of the total transport ψ_I is 15.2 Sv whereas the actual ψ_I is 12.6 Sv.

In Fig. 8b the situation is identical except that the Δ has been decreased to 400 km. The band of reverse (southward) flow in the gap has been eliminated and the total transport has increased to 16.3 Sv. Although the island rule also predicts an increase in transport (to 17.4 Sv), it is proportionally smaller than the actual increase. (The reason that the island rule predicts a transport increase is that some of the southward flow in the $\Delta = 600$ km gap is Sverdrup transport. Moving the island westward cuts down on the southward Sverdrup transport in the gap and, at the same time, increases the southward Sverdrup transport to the *east* of the island, rendering a larger total anticyclonic transport around the island.)

Finally, Fig. 8c shows the effects of increasing nonlinearity in the Fig. 8a setting, though not to the point of making the flow unsteady. Here δ_I has been increased from 20 to 100 km resulting in a north–south asymmetry. The transports here are unrealistically large (380 Sv predicted by the island rule and 312 Sv calculated numerically) but the ratio of actual to island rule transport is nearly the same as in the linear counterpart (Fig. 8a). This result is consistent with the findings of PPSH that it is mainly friction and not nonlinearity that accounts for departures from the island rule.

Figures 9a and 9b show actual ψ_I, normalized by the

[2] Some exceptions occur when the island dimensions are as small as the boundary layer thickness δ_M. In this case, however, *all* the dissipation terms are small and the island rule reduces to the Sverdrup relation.

[3] Readers familiar with PPSH might remark on the absence of a closed recirculation along the eastern boundary of the island. Such a feature is possible when the wind stress curl reaches an extreme value within the latitude band of the island, as ours does, and *always* occurs under this condition when the island thickness L is zero. The lack of a closed recirculation here is due, among other things, to the substantial contribution of the wind stress along the northern and southern boundaries of the island in (1.1).

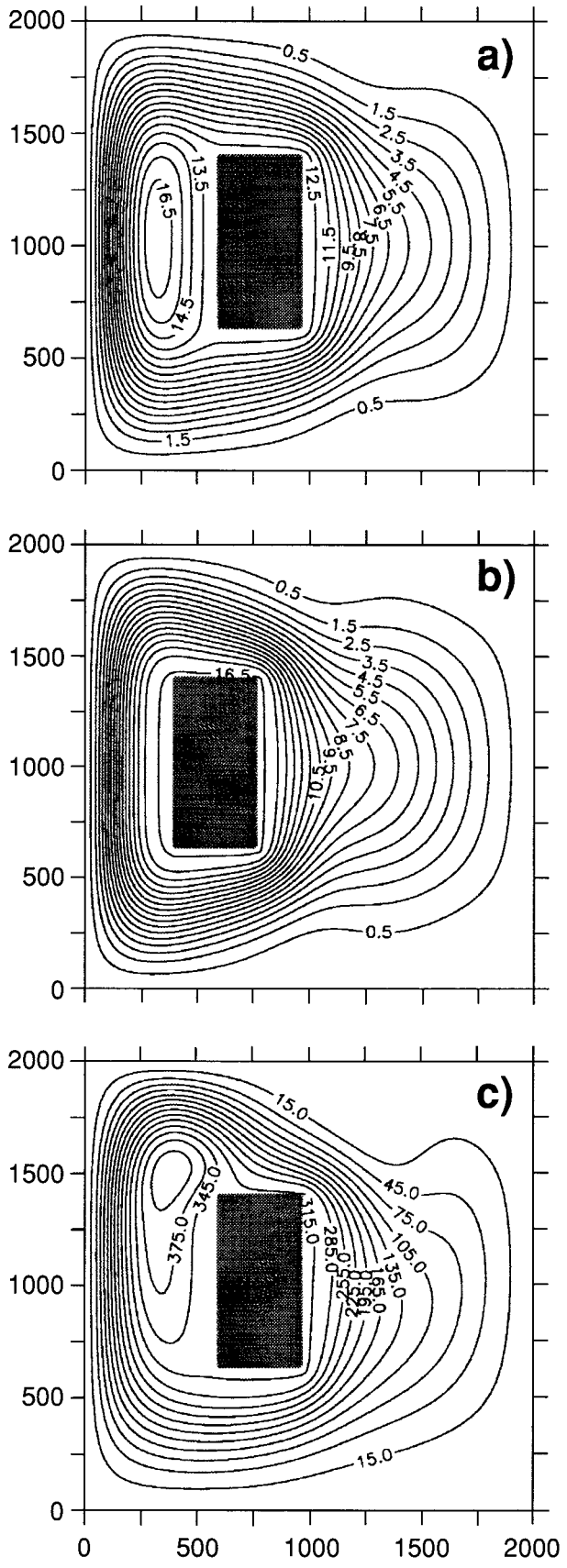

corresponding original island rule ψ_I, for several sequences of experiments in which the island is brought successively closer to the western boundary. Figure 9a summarizes the results for experiments using the Fig. 8 island and forcing, with the open circles representing the ''linear'' case $\delta_I/\delta_M = 0.2$ and the solid dots representing the ''nonlinear'' case ($\delta_I/\delta_M = 1.0$). As noted by PPSH, nonlinearity does not lead to significant changes in the (normalized) transport.[4] The transport given by the original island rule (1.2) is indicated by the horizontal line and the transport predicted by the extended island rule (3.7) is indicated by the curve. For the experiments summarized in Fig. 9b, all parameters are unchanged except that the island is now only 180 km by 180 km and only the linear setting $\delta_I/\delta_M = 0.2$ is explored. This smaller island was analyzed to evaluate the effect of making the gap less oblong and thereby worsening the approximation $\partial/\partial x \gg \partial/\partial y$.

When the island is well separated from the western boundary ($\Delta/\delta_M > 3$) the transports are within 75% of the value predicted by the island rule, and this is consistent with the findings of PPSH. As the island is moved within several values of δ_M of the western boundary, the transport temporarily increases, then decreases, as predicted. For smaller separations the transport is reduced well below the island rule value. Agreement with the extended island rule is very good in most cases. One exception occurs in the case of the smaller island (Fig. 9b) when $\Delta/\delta_M = 8$, where the improvement over the original island rule is only marginal.

5. Comparison with island western boundary layer transport

To an investigator of field cases, the primary unknown removed by the island rule is not the total transport but rather the transport in the island's western boundary current. That is, the Sverdrup component of the circulation between the island and the basin's eastern boundary can always be computed without any reference to the island, and the only component left is the western boundary layer transport. This idea can be formalized by setting

[4] Equation (1.1) shows that violations of the island rule due to nonlinearity arise in the form of relative vorticity fluxs $\mathbf{u}\cdot\zeta d\mathbf{n}$. One expects that these fluxes will be largest in the island's western boundary layer, where $\mathbf{u}\cdot\zeta d\mathbf{n} \simeq v\partial v/\partial x$. However, the integral of the latter across the eastern gap vanishes due to the no-slip boundary conditions. The meridional flow in the gap therefore has zero net vorticity flux to lowest order.

←

FIG. 8. Steady streamfunction contours obtained from a barotropic version of the MICOM model with the anticyclonic wind stress curl distribution shown in Fig. 2 and with $\delta_I = 20$ km and $\delta_M = 100$ km. The gap thicknesses are (a) $\Delta = 600$ km, (b) $\Delta = 400$ km, and (c) $\Delta = 600$ with δ_I increased to 100 km.

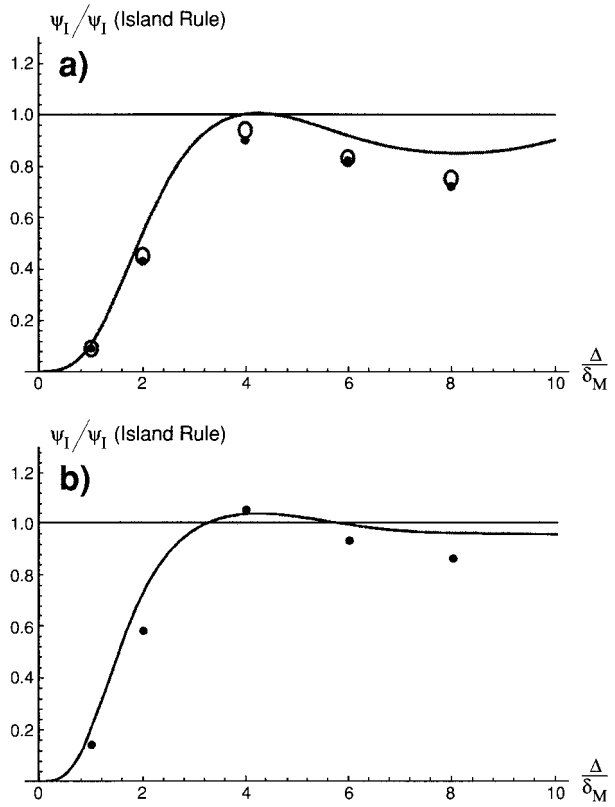

FIG. 9. The total transport around the island ψ_I, normalized by the transport predicted by the island rule, as a function of dimensionless gap width. The open circles show values from numerical simulations with $\delta_M = 100$ km and $\delta_I = 20$, while δ_I has been increased to 100 km for the solid dots. The horizontal line shows the value predicted by the original island rule (1.2) while the curve shows the values predicted by the extended island rule (3.7). The results pertain to the (a) larger 380 km by 780 km island and (b) the smaller 180 km by 180 km island.

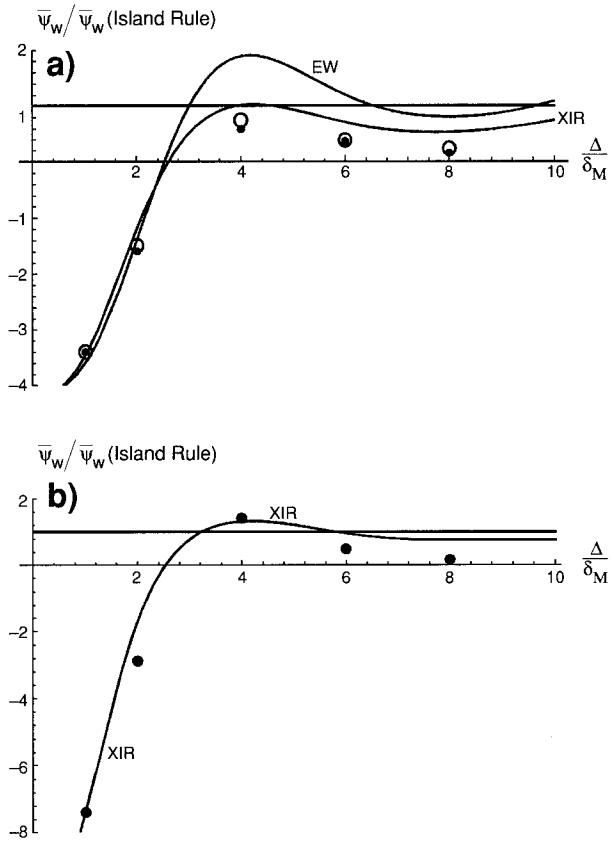

FIG. 10. Same as Fig. 8 except the transports shown are the average transports in the western boundary layer on the island's east coast, normalized by the western boundary layer transport predicted by the original island rule. The curves labled XIR correspond to the extended island rule [Eq. (3.7)] while the curve in (a) marked EW shows the theoretical value obtained by considering friction only in the gaps [see Eq. (2.10)].

$$\psi_I = \overline{\psi}^S + \overline{\psi}_W,$$

where $\overline{\psi}^S$ represents the meridional average over $y_N < y < y_S$ of the total Sverdrup transport between the island and the eastern basin boundary, and $\overline{\psi}_W$ is the meridional average of the western boundary layer transport. Then $\overline{\psi}_W$ may be considered the fundamental unknown.

Figures 10a and 10b are identical to 9a and 9b except that $\overline{\psi}_W$ is used as the basis for comparison. When the island is well separated from the western basin boundary, the measured $\overline{\psi}_W$ (dots and circles) now differ from the island rule $\overline{\psi}_W$ (horizontal line) by as much as 85%. This error is somewhat larger than that observed by PPSH due to the larger value of δ_M used here (100 km compared to the 40 and 20 km used by PPSH). Of course, this error is only important when $\overline{\psi}_W$ constitutes a significant portion of $\overline{\psi}_I$, a matter that must be judged on a case-by-case basis. When $\overline{\psi}_W$ is not a significant portion of the total, use of the island rule is probably not required to begin with.

The solid curves labled XIR in Figs. 10a and 10b correspond to $\overline{\psi}_W$ predicted by the extended island rule (3.7) and are obtained from that equation by subtracting

$$\overline{\psi}^S = \frac{-\oint_{C'} (\boldsymbol{\tau}/\rho)\cdot\mathbf{t}\, ds}{\beta(y_N - y_S)}$$

from the right-hand side. Here C' is the contour enclosing the ocean area to the east of the island. For gap thicknesses $\Delta/\delta_M \leq 4$, the numerical values of $\overline{\psi}_W$ are well predicted by this formula, with errors less than about 20% in all but one case. For wider gaps, the impovement over the original island rule is good to fair. Finally, the curve labeled EW in Fig. 10a represents Eq. (2.12), which accounts for friction in the gap but not on the north or south boundaries of the island. As expected, the error in neglecting the north–south boundary friction is noticable only for gaps wider than about $3\delta_M$.

6. Stommel model

Construction of an extended island rule for Stommel flow with bottom friction proceeds from (2.1) in the same manner as before. The flow field is composed of Sverdrup interior regions, Stommel layers on east-facing boundaries, and diffusive layers on the north and south coasts of the island. The Stommel layer contains no recirculation and, in contrast to the Munk model, there is no increase in the value of ψ_I (relative to the original island rule value) as the gap is narrowed. Derivation of the dissipation terms D_E, D_W, etc., is described in the appendix. After substitution into (2.1) and some rearrangement, the following extended rule is obtained:

$$\psi_I = \frac{-\oint_C (\boldsymbol{\tau}/\rho)\cdot\mathbf{t}\, ds - \kappa_S\left(\frac{2}{3}L + \Delta_E\right)[\mathrm{curl}(\boldsymbol{\tau}/\rho)_{y=y_N} + \mathrm{curl}(\boldsymbol{\tau}/\rho)_{y=y_S}] - D_S}{\beta\{(y_N - y_S)[(1 - e^{-\Delta/\delta_S})^{-1} + (e^{-\Delta_E/\delta_S} - 1)^{-1}] + 2\kappa_S\}}, \tag{6.1}$$

where $\kappa_S = 2(\delta_S L)^{1/2}/\sqrt{\pi}$, $\delta_S = D_f/\beta H$ in which D_f is a linear bottom drag coefficient, and D_S is given by Eq. (A.6).

If the gap to the east or west of the island is tilted at a small angle, θ, with respect to y (but sill has constant width), one can formulate a rule similar to (6.1) or (3.7) by replacing β by $\beta\cos\theta$ in those dissipation terms effected. For example, if the gap to the west of the island is tilted, one would make this replacement in the dissipation term D_W, as defined by (2.7) for the Munk model or by (A.2) for the Stommel model. This situation is discussed by Wajsowicz (1993).

7. Discussion and application to the Indonesian Throughflow

A limitation in the application of our results to real ocean islands is that (3.7) or (6.1) requires knowledge of the dissipative length scales δ_M or δ_S, both of which are known only within broad ranges. As an example of what can and cannot be said about specific islands and gaps, consider the throughflow of the Indonesian seas (Fig. 2). The bulk of the Pacific-to-Indian Ocean transport is thought to cross the equator in the Makassar Strait (sill depth $\approx$ 550 m, minimum width $\approx$ 120 km) with a smaller portion passing through gaps of similar width in the Ceram and Molucca Seas to the east (e.g., Kindle et al. 1989; Masumoto and Yamagata 1996; Metzger and Hurlburt 1996). According to Wyrtki, the primary choke point for the eastern component of the flow is the Lifamatola Strait (sill depth $\approx$ 2000 m, width $\approx$ 90 km). Farther to the south, the flow encounters the Indonesian archipelago where it must filter through even thinner gaps. According to Molcard et al. (1996) the transport is carried in three main branches. Two occur in the Lombok Strait (minimum width $\approx$ 20 km, sill depth $\cong$ 300 m) and the Ombai Strait (minimum width $\approx$ 30 km, sill depth $\approx$ 1100 m), both labeled in Fig. 2. The third branch had been directly measured south of Timor (Molcard et al. 1996) and filters through straits lying to the east, and perhaps north, of Timor. The maximum width of these straits is about 100 km, but the distribution of flow is unknown.

Although the throughflow is not barotropic, the bulk of the transport is thought to be confined to the upper 200–300 m (Wyrtki 1961; Murray and Arief 1988; Fieux et al. 1994). An equivalent barotropic model with active upper layer and inactive lower layer might therefore serve as a good first approximation to the flow. As pointed out earlier, the results derived herein are equally valid (under linear conditions) for an equivalent barotropic model. Of the straits mentioned above, only the Lombok has a sill as shallow as 300 m, and we will therefore focus on lateral friction, rather than bottom friction, as a possible blocking mechanism.

According to the theoretical and numerical results presented herein, significant blocking of a throughflow will occur when the gap thickness Δ becomes less than about $3\delta_M$. Based on published estimates of the value of the horizontal eddy viscosity (Bryan 1987; Brown and Owens 1981), δ_M ranges from 10 to 100 km. However, the observed widths of western boundary layers are rarely less than 100 km, as can be verified by examining hydrographic sections across the Gulf Stream, Kuroshio, Malvinas, Agulhas, and Brazil Currents.[5] It is certainly possible that this 100 km represents an inertial length scale $\delta_I = (U/\beta)^{1/2}$, where U is a velocity scale based on the Sverdrup interior. However, even an optimistically large U of 2 cm s^{-1} yields $\delta_I \leq 35$ km for mid- or low-latitude values of β. So it is quite possible that observed larger thicknesses reflect a frictional process. Indeed, the absence of observations of surface western boundary layer thickness as small as 35 km argues that we consider the upper range of estimates of δ_M. Since the decay scale of the Munk profile is $2\delta_M$, a conservative choice would be $\delta_M = 50$

[5] The references to such sections are too numerous to be mentioned. However, a fine reference list appears in the review paper of Hogg and Johns (1995).

km, or half the typical minimum observed thickness. This value also lies in the middle of the possible range based on eddy viscosity estimates. The value of Δ below which frictional blocking would occur is then three times the minimum value in this range, or 150 km. The latter is indicated by the longer bar in the lower, left-hand portion of Fig. 2. It is greater than the width of the thinnest gap through which any branch of the Indonesian Throughflow must pass. Also indicated in Fig. 3 is a smaller bar having a length of 30 km, which is $3\delta_M$ for the smallest δ_M (=10 km) suggested by eddy viscosity estimates. This value is larger than the minimum widths of the Ombai and Timor passages but not the other passages mentioned above.

The original island rule assumes negligible dissipation on the western boundary of the island, which in turn requires that the gap to the west of the island be sufficiently large. Other islands and gaps may exist far to the west of the island but these are of no consequence as long as the gap to the immediate west of the island is large. As pointed out by Wajsowicz (1996), the entire flow to the west of the island may pass through the smaller gaps and may experience local dissipation, but this does not invalidate the island rule. In the case of the Indonesian Throughflow, it might be possible to find a path through the Indonesian seas that avoids passing through any gap narrower than $3\delta_M$. In Fig. 2, such a path might follow the Lifamatola Strait southward and then pass through one of the straits to the east of Timor. Suppose that the gaps farther to the east (such as the passages to the east of Halmahera) are much smaller than $3\delta_M$. Then the magnitude of the throughflow could be estimated by applying the island rule along a contour that hugs the coastlines immediately to the east of the path. (Note that the throughflow itself would not necessarily follow this path.) This estimate would obviously miss any transport passing through the minor gaps lying to the east of Halmahera. In any case, the range in the above estimates of δ_M make it difficult to determine whether such a path exists.

In summary, midpoint estimates for δ_M suggest lateral friction as a serious candidate for the overestimate of the Indonesian Throughflow transport by Godfrey's island rule. Estimates of δ_M in the lower range of acceptable values suggest frictional impedance in the Lombok and Ombai Straits, but not necessarily the straits to the east of Timor. In this case, evaluation of frictional effects must await better observations of the partitioning of these three branches of the throughflow. Also, there certainly are other influences, such as bottom topography and baroclinicity, which may lead to departures from the original island rule.

One can apply the same ideas to assess the strength of friction in other oceanographically important gaps. For example, the Mozambique Channel (between Africa and Madagascar) is >300 km wide for depths >200 km. It is therefore unlikely that the western edge of Madagascar experiences much dissipation, implying that the original island rule may apply. Quite the opposite is true for the 20-km-wide English Channel, which by the above estimates, must experience significant dissipation on its eastern side. With depths generally <200 m, the English Channel also must experience significant dissipation due to bottom friction. In fact, a typical bottom drag coefficient $D_f = 5 \times 10^{-4}$ m s^{-1} combined with a bottom depth scale $H = 100$ m gives a Stommel boundary layer thickness $\delta_S = D_f/\beta H = 250$ km. According to (6.1) dissipation due to bottom friction should come into play when the gap thickness is $\geq \delta_S$, and this condition seems well satisfied. The Denmark Strait is harder to judge due to the extreme topographic variations. There is a central trough with depths >500 m, which narrows to about 30 km, and lateral friction could be significant for the flow confined to this trough. The wetted width of the strait is about 800 km, much of it occupied by depths ranging from 100 to 500 m. The Stommel thickness corresponding to $D_f = 5 \times 10^{-4}$ m s^{-1} ranges from 50 to 250 km over this depth, and it is therefore less likely that bottom friction would cause a serious violation of the island rule.

Acknowledgments. This work was carried with the support of the National Science Foundation under Grants OCE-9520302 and OCE-9502083. The authors would like to thank Nancy Bray, Karl Helfrich, Susan Hautala, Doron Nof, and Mike Spall for a number of helpful suggestions.

APPENDIX

The Extended Island Rule for Flow with Bottom Friction

The procedure for calculating the dissipation terms D_W, D_N, etc., in (2.1) is similar to that used for the Munk problem. In the gap to the west of the island, the flow is governed by

$$\frac{\partial^2 \psi}{\partial x^2} + \delta_S^{-1} \frac{\partial \psi}{\partial x} = H D_f^{-1} \mathrm{curl}\left(\frac{\boldsymbol{\tau}}{\rho}\right), \tag{A.1}$$

(Pedlosky 1996). Here D_f is the bottom drag coefficient and $\delta_S = D_f/\beta H$ is the Stommel western boundary layer thickness. Also, the dissipation is now proportional to the tangential velocity along along the solid wall:

$$\mathrm{diss}(\mathbf{u}) = -D_f \mathbf{u}/H.$$

Solving (A.1) subject to the boundary conditions $\psi = 0$ at $x = 0$ and $\psi = \psi_I$ at $x = \Delta$ and using the solution to evaluate the dissipation along the west coast of the island leads to

$$\begin{aligned} D_W &= D_f \int_{y_S}^{y_N} v(\Delta, y)\, dy \\ &= \frac{\beta(y_N - y_S)\psi_I}{(e^{\Delta/\delta_S} - 1)} + \frac{D_f}{\beta H^2}\left[1 - \frac{\Delta}{\delta_S(e^{\Delta/\delta_S} - 1)}\right] \\ &\quad \times \int_{y_S}^{y_N} \mathrm{curl}(\boldsymbol{\tau}(\Delta, y)/\rho)\, dy, \end{aligned} \tag{A.2}$$

where the wind stress is assumed to be x independent. The first term on the right-hand side of (A.2) was obtained by Wajsowicz 1993 [see her Eq. (4.2)] by solving the homogeneous version of (A.1). The second term reflects the effects of Sverdrup flow in the gap and is likely to be significant only for wide gaps. In the gap to the east of the island a similar calculation gives

$$D_E = \frac{\beta(y_N - y_S)\psi_I}{(e^{\Delta_E/\delta_S} - 1)} - \frac{D_f}{\beta H^2}\left[1 - \frac{\Delta_E}{\delta_S(e^{\Delta_E/\delta_S} - 1)}\right] \times \int_{y_S}^{y_N} \text{curl}(\boldsymbol{\tau}(L_B, y)/\rho)\, dy. \quad \text{(A.3)}$$

As in the Munk problem, the flow along the north and south island coasts is contained in a diffusive layer. This layer is analyzed by PPSH, and the boundary layer solution [their Eq. (2.34)] can be used to calculate the dissipation terms

$$D_N = \beta\kappa_S\psi_I + \kappa_S\left(\frac{2}{3}L + \Delta_E\right)\text{curl}\left(\frac{\boldsymbol{\tau}}{\rho}\right)_{y=y_N} \quad \text{(A.4)}$$

$$D_S = \beta\kappa_S\psi_I + \kappa_S\left(\frac{2}{3}L + \Delta_E\right)\text{curl}\left(\frac{\boldsymbol{\tau}}{\rho}\right)_{y=y_S}, \quad \text{(A.5)}$$

where $\kappa_S = 2(\delta_S L)^{1/2}/\sqrt{\pi}$.

After substitution of all dissipation terms into (2.1) and some rearrangement, the following extended rule (6.1) is obtained. In the latter, the following shorthand is used:

$$D_S = \frac{D_f}{\beta H^2}\left[1 - \frac{\Delta}{\delta_S(e^{\Delta/\delta_S} - 1)}\right]\int_{y_S}^{y_N} \text{curl}(\boldsymbol{\tau}(\Delta, y)/\rho)\, dy - \frac{D_f}{\beta H^2}\left[1 - \frac{\Delta_E}{\delta_S(e^{\Delta_E/\delta_S} - 1)}\right]\int_{y_S}^{y_N} \text{curl}(\boldsymbol{\tau}(L_B, y)/\rho)\, dy. \quad \text{(A.6)}$$

REFERENCES

Bleck, R., C. Rooth, D. Hu, and L. T. Smith, 1992: Salinity-driven thermocline transients in a wind- and thermohaline-forced isopycnal coordinate model of the North Atlantic. *J. Phys. Oceanogr.*, **22,** 1486–1505.

Brown, E. D., and B. Owens, 1981: Observations of the horizontal interactions between the internal wave field and the mesoscale flow. *J. Phys. Oceanogr.* **11,** 1474–1480.

Bryan, K., 1969: A numerical study of the circulation of the world ocean. *J. Comput. Phys.*, **4,** 347–376.

——, 1987: Potential vorticity in models of the ocean circulation. *Quart. J. Roy. Meteor. Soc.*, **113,** 713–734.

Erdelyi, A., W. Magnus, F. Oberhettinger, and F. G. Tricomi, 1954: *Tables of Integral Transforms.* McGraw-Hill, 391 pp.

Fieux, M., C. Andrie, P. Delecluse, A. G. Ilahude, A. Kartavtseff, F. Mantisi, R. Molcard, and J. C. Swallow, 1994: Measurements within the Pacific–Indian Ocean throughflow region. *Deep-Sea Res.*, **41,** 1091–1130.

Godfrey, J. S., 1989: A Sverdrup model of the depth-integrated flow from the world ocean allowing for island circulations. *Geophys. Astrophys. Fluid Dyn.*, **45,** 89–112.

Hogg, G., and W. E. Johns, 1995: Western boundary currents. *Rev. Geophys. Suppl.*, 1311–1334.

Kamenkovitch, V. M., 1962: *Trudy Instituta Okeanologii.* Akad. Nauk SSSR, **56,** 241 pp.

Kindle, J. C., H. E. Hurlburt, and E. J. Metzger, 1989: On the seasonal and interannual variability of the Pacific-Indian Ocean throughflow. *Proc. Western Pacific Int. Meeting and Workshop on TOGA-COARE*, Noumea, New Calidonia, ORSTROM, 355–366.

Masumoto, Y., and T. Yamagata, 1996: Seasonal variations of the Indonesian throughflow in a general circulation model. *J. Geophys. Res.*, **101** (C5), 12 287–12 294.

Metzger, E. J., and H. E. Hurlburt, 1996: Coupled dynamics of the South China Sea, the Sulu Sea, and the Pacific Ocean. *J. Geophys. Res.*, **101** (C5), 12 331–12 352.

Molcard, R., M. Fieux, and A. G. Ilahude, 1996: The Indo–Pacific throughflow in the Timor Passage. *J. Geophys. Res.*, **101** (C5), 12 411–12 432.

Murray, S. P., and D. Arief, 1988: Throughflow into the Indian Ocean through the Lombok Strait, January 1985–January 1986. *Nature*, **333,** 444–447.

Pedlosky, J., 1996: *Ocean Circulation Theory*. Springer-Verlag, 453 pp.

——, L. J. Pratt, M. A. Spall, and K. R. Helfrich, 1997: Circulation around islands and ridges. *J. Mar. Res.*, **55,** 1199–1251.

Qiu, B., D. Koh, C. Lumkin, and P. Flament, 1997: On the existence and formation mechanism of the North Hawaiian Ridge Current. *J. Phys. Oceanogr.*, **27,** 431–444.

Wajsowicz, R. C., 1993: The circulation of the depth-integrated flow around an island with applications to the Indonesian Throughflow. *J. Phys. Oceanogr.*, **23,** 1470–1484.

——, 1996: Flow of a western boundary current through multiple straits: An electrical circuit analogy for the Indonesian throughflow and archipelago. *J. Geophys. Res.*, **101,** 12 295–12 300.

Wijffels, S. E., N. Bray, S. Hautala, G. Meyers, and W. M. L. Morawitz, 1996. The WOCE Indonesian throughflow repeat hydrography sections: I10 and IR6. *Int. WOCE Newslett.*, **24,** 25–28.

Wyrtki, K., 1961: Scientific results of marine investigation of the South China Sea and the Gulf of Thailand, 1959–1961, Vol. 2, *Physical Oceanography of Southeast Asian Waters*. Scripps Inst. of Oceanogr. NAGA Rep. 2, University of California, San Diego, CA, 195 pp.